Acc. Chem. Res. **2000,** *33,* 457−466

Nanofabrication of Self-Assembled Monolayers Using Scanning Probe Lithography

GANG-YU LIU,* SONG XU, AND YILE QIAN
Department of Chemistry, Wayne State University, Detroit, Michigan 48202

Received September 16, 1999

ABSTRACT
This Account focuses on our recent and systematic effort in the development of generic scanning probe lithography (SPL)-based methodologies to produce nanopatterns of self-assembled monolayers (SAMs). The key to achieving high spatial precision is to keep the tip−surface interactions strong and local. The approaches used include two AFM-based methods, nanoshaving and nanografting, which rely on the local force, and two STM-based techniques, electron-induced diffusion and desorption, which use tunneling electrons for fabrication. In this Account we discuss the principle of these procedures and the critical steps in controlling local tip−surface interactions. The advantages of SPL will be illustrated through various examples of production and modification of SAM nanopatterns and their potential applications.

Introduction

Microfabrication of self-assembled monolayers (SAMs) has attracted tremendous attention because patterned SAMs can be used as resists for pattern transfer[1−3] and as templates to pattern proteins and other biosystems.[4] Micrometer-sized patterns have been fabricated within SAMs using microlithographic techniques such as photolithography,[5] microcontact printing,[2,6−8] microwriting,[2,6,8] and micromachining.[8] Argon ion or electron beam lithography can produce smaller patterns (down to tens of nanometers) but require a high-vacuum environment.[9] Another approach to produce nanometer-sized domains of SAMs is the coadsorption of two or more adsorbates.[10,11] However, with this approach, it is difficult to precisely control the size and distribution of these nanodomains because the structure is determined by the interplay of the kinetics and thermodynamics of the self-assembly process.[10,11]

Creating nanopatterns of SAMs with molecular precision requires new fabrication strategies. Scanning probe microscopy (SPM) techniques such as scanning tunneling microscopy (STM)[12] and atomic force microscopy (AFM)[13] are well-known for their ability to visualize surfaces of materials with the highest spatial resolution.[14] Taking advantage of the sharpness of the tips, and strong and localized tip−surface interactions, SPM has also been used to manipulate atoms on metal surfaces and to fabricate nanopatterns of metal and semiconductor surfaces.[15,16] These successful examples catalyze an emerging field of scanning probe lithography (SPL). Recent progress in SPL of various materials has been discussed in several reviews.[17,18] Complementary to those studies, our research interests focus on SPL of SAMs.

Despite the structural complexity of SAMs, molecular resolution images have been obtained using both AFM[19,20] and STM.[21,22] The fact that molecules within SAMs can be resolved indicates that the tip−SAM interaction in AFM imaging and the tunneling electrons in STM imaging are localized to molecular dimensions. Therefore, in principle, by enhancing these local interactions such as force, density of tunneling electrons, or electrical field strength, one is able to break chemical bonds selectively. The detailed methodology in controlling these local interactions is the key to obtaining sharp patterns with high spatial precision. Various approaches of controlling the local interactions have been reported. These methods include AFM-based lithography such as tip-catalyzed surface reactions,[23] dip-pen nanolithography,[24] and STM-based lithography such as tip-assisted electrochemical etching and field-induced desorption.[25]

In this Account, we focus on our recent and systematic efforts in developing generic SPL-based methodologies to produce nanopatterns of SAMs. We first discuss the principle of our SPL procedures. The critical steps in controlling local tip−surface interactions will then be addressed. The advantages of our approach will be illustrated through various examples of production and modification of SAM nanopatterns. Finally, we introduce our preliminary studies on some promising applications of nanofabrication of SAMs using SPL.

Methodology of Nanofabrication of SAMs Using SPL

Basic Procedures. The highest resolution AFM images of thiol SAMs were acquired in liquid media under very low

Gang-yu Liu received her B.Sc. in chemistry at Peking University (China) in 1985, followed by a Ph.D. in chemistry in 1992 from Princeton University under the supervision of Professor Giacinto Scoles. From 1992 until 1994, she was a Miller Research Fellow at the University of California at Berkeley with Dr. Miquel Salmerson and Professor Y. T. Lee. She joined Wayne State University in 1994 as an Assistant Professor and was promoted to Associate Professor of Chemistry with tenure in 1999. Her research interests include nanofabrication techniques, size-dependent physical properties and chemical reactivities of materials with nanometer dimension, nanoelectronic devices, and biosensor and biochip fabrication.

Song Xu received his B.Sc. in chemistry from the University of Science and Technology of China in 1991. He spent the following three years at the Central Laboratory of Suzhou University as a research staff member working in Magnetic Material and Mossbauer Spectroscopy. He is currently completing a Ph.D. degree with Gang-yu Liu at the Department of Chemistry, Wayne State University. His research interests include the development of nanofabrication techniques and scanning force microscopy instrumentation.

Yile Qian received his B.Sc. in applied physics from Hefei University of Technology of China in 1982, and M.Sc. in physics from Anhui Institute of Optics & Fine Mechanics in 1988 under the supervision of Professor Chunkai Wu. He remained at the Institute from 1988 until 1994 as a research staff member working in the area of molecular beam and laser spectroscopy. After spending one year as visiting scholar at Theoretical & Physical Chemistry Institute (NHRF, Grace), he came to Wayne State University in 1995, and is currently a Ph.D. candidate with Gang-yu Liu. His research focuses on nanofabrication methodology, scanning tunneling microscopy, and nanoelectronic devices.

10.1021/ar980081s CCC: $19.00 © 2000 American Chemical Society
Published on Web 03/16/2000

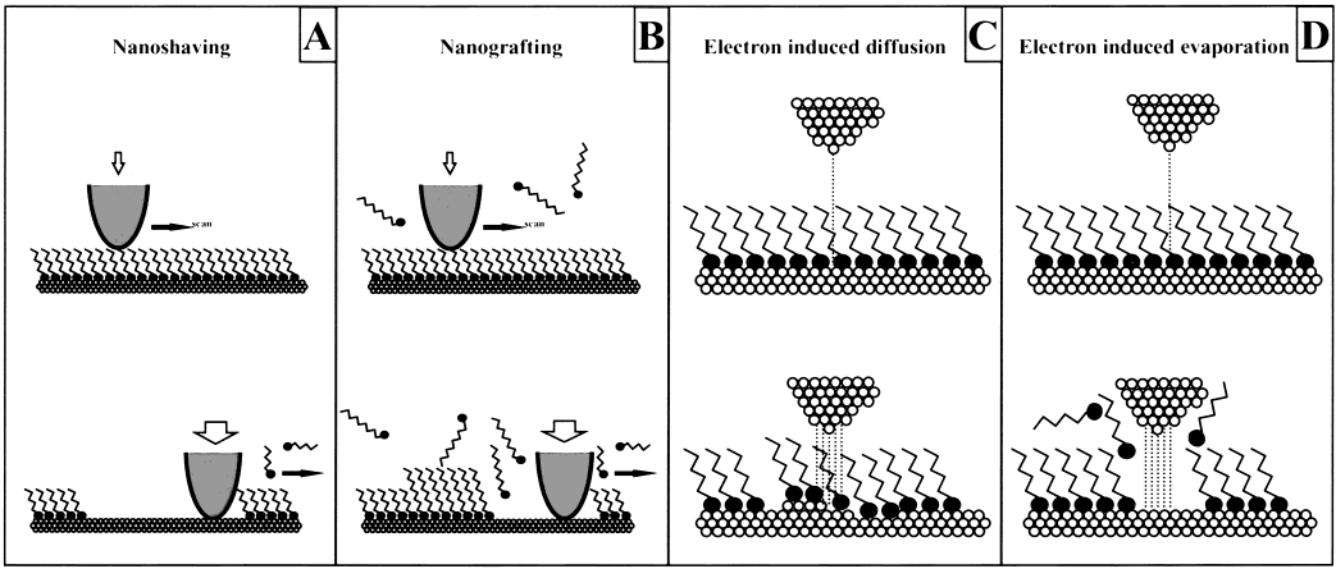

FIGURE 1. Schematic diagrams of four basic manipulation mechanisms using AFM (A and B) and STM (C and D). The imaging and fabrication modes are depicted in the top and bottom rows, respectively.

imaging forces (e.g., 0.05 nN).[19,20] The pressure exerted by the tip was ~0.01 GPa (assuming a tip radius of ~100 Å). The van der Waals energy per CH_2 group is ~2 kcal/mol.[26] Therefore, under such imaging pressure, the AFM tip was in contact with the alkane chains, which causes small local deformation.[26] Increasing the local pressure would increase the deformation, disrupt the packing, and eventually displace thiol molecules from their adsorption sites because the Au−S bond is the weakest at the interface (the binding energies for S−Au, C−C, C−H, and C−S are 40, 145, 81, and 171 kcal/mol, respectively). In addition, the lateral movement of thiols on gold requires less activation energy than desorption. Increasing the load further would cause the underlying gold substrate to deform.

The procedure of our AFM-based lithography is illustrated in Figure 1A,B. First, the surface structure is characterized under a very low force or load. Fabrication locations are normally selected in regions with flat surface morphology, e.g., Au(111) plateau areas. The second step is patterning SAMs under high force. In nanoshaving (Figure 1A, bottom), the AFM tip exerts a high local pressure at the contact. This pressure results in a high shear force during the scan, which causes the displacement of SAM adsorbates. There is a distinct difference between nanoshaving and wearing.[26] In nanoshaving, adsorbate molecules are displaced by an AFM tip during the scan at a load higher than the displacement threshold.[27] Holes and trenches can be fabricated with one scan. Wearing is normally referred to as the detaching of adsorbates by repeated scanning of an AFM tip under a load smaller than the threshold.[26] In wearing, molecules are gradually moved away from the edges of defect sites. During AFM scans, both processes may occur simultaneously, although shaving is the dominant process under high load.

In nanografting (Figure 1B), AFM tips are also used to shave thiol molecules from their adsorption sites.[28] The SAM and the AFM cantilever are immersed in a solution containing a different thiol. The thiol molecules in the solution adsorb on the newly exposed gold surface as the AFM tip plows through the matrix SAM. The nanostructures are characterized in the third step at reduced loads (top panels in Figure 1A,B).

In STM-based lithography, tunneling electrons are used to achieve nanofabrication of SAMs. As illustrated in Figure 1C,D, SAMs are first imaged under a very low tunneling current, and then fabrication locations are chosen. Unlike in AFM, STM tips are not in contact with the surface during imaging. Under ultrahigh vacuum (UHV), the tunneling current is slowly increased while the bias voltage is maintained constant. As the tunneling current is increased beyond a certain threshold, displacement of metal atoms or desorption of adsorbate molecules occurs (bottom panels in Figure 1C,D). The resulting patterns can then be imaged at a reduced current.

Determination of the Threshold Force and Current. Fabrication force and current are the key parameters in maintaining a local tip−surface interaction. Extremely high forces in AFM can cause plastic deformation or displacement of the underlying gold substrate.[29] On the other hand, if the force is too low, molecules cannot be displaced completely in one scan. Multiple scans could result in winding edges due to the drift between scans. Since the fabrication threshold varies with the geometry of AFM tips, the structure of the matrix SAMs, and the fabrication environment, the threshold should be determined in situ for each individual experiment before attempting fabrication.

The force threshold can be determined by monitoring the changes in surface structure as a function of increasing load. The structural changes are best monitored from molecular resolution images taken at relatively small scanning areas (typically, 3×3 to 25×25 nm^2). Under low imaging forces, topographic images reveal the molecular packing within SAMs. Figure 2A,C shows an

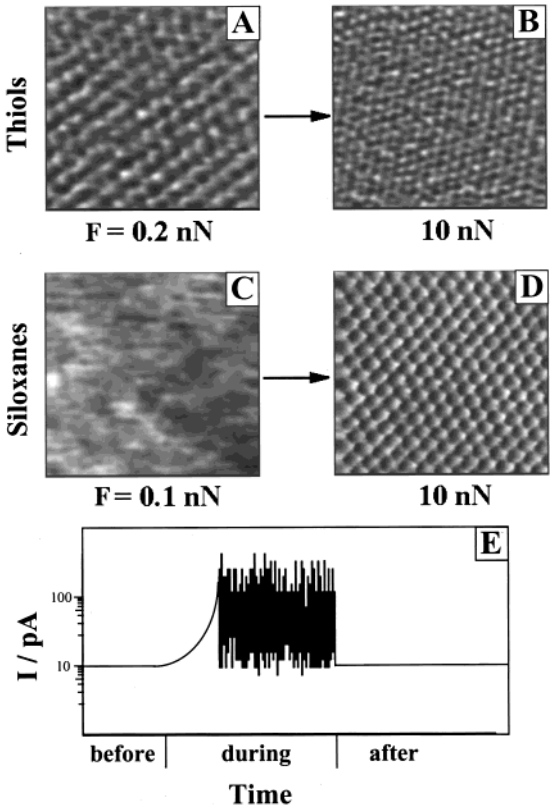

FIGURE 2. Determination of threshold force and tunneling current. Topographic images (5 × 5 nm^2) of (A) C_{18}S/Au(111) and (C) OTE/mica taken in 2-butanol. At a load of 10 nN, images A and C changed into the periodicity of (B) Au(111) and (D) mica (0001), respectively. The threshold forces are 9.5 and 9.6 nN, respectively, which correspond to a pressure of 0.4 GPa based on the Hertzian model. (E) Sudden fluctuation occurs when the tunneling current causes diffusion or displacement.

ordered octadecanethiol monolayer on gold (abbreviated as C_{18}S/Au) and a disordered octadecyltriethoxysilane layer on mica (OTE/mica), respectively. As the load increases, the images remain unchanged at first and become increasingly distorted at higher forces. A continuous increasing of the imaging force results in a transition in the AFM image from the lattice of SAM to that of the substrate. Figure 2B,D reveals that both Au(111) and mica (0001) have a hexagonal symmetry with lattice constants of 2.88 and 5.18 Å, respectively. The load at which the transition occurs is referred to as the displacement threshold. In the experiments shown in Figure 2, the displacement thresholds for C_{18}S/Au and OTE/mica are 9.5 and 9.6 nN, respectively.

At fixed bias voltage, the tunneling current in STM increases exponentially with decreasing tip−surface distance.[12,14] At high current, STM tips may become attached to the surface, resulting in nonlocal fabrication such as the formation of deep pits or irregularly shaped clusters. Very often, tips become very dull upon separation due to removal of or picking up of materials. To determine the threshold current, we first optimize the imaging conditions for SAMs, i.e., the bias voltage (V) and tunneling current (I). Typical V and I values for decanethiol SAM are ±1 V and 5−15 pA, respectively.[21,22] Keeping the voltage constant, we gradually increase the current by moving the tip toward the surface. As illustrated in Figure 2E, a large fluctuation in I is observed when the current reaches the fabrication threshold. The fluctuation is attributed to movements of atoms and molecules under the tip.

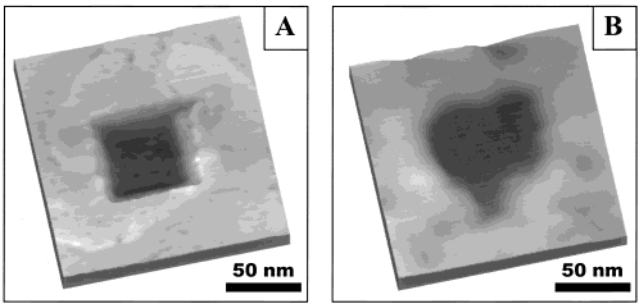

FIGURE 3. (A) 160 × 160 nm^2 topographic images of C_{18}S/Au(111) with the thiols shaved away from the central 50 × 50 nm^2 square. (B) 160 × 160 nm^2 topographic images of OTE/mica containing a heart-shaped pattern produced using nanoshaving.

Nanopatterning of SAMs Using SPL

Nanoshaving. There are a number of requirements to produce sharp nanopatterns using nanoshaving: local displacement, immediate removal of the displaced adsorbate, and absence of readsorption. The fate of the displaced molecules depends on the structure of SAMs and the fabrication environment. Alkane thiols form an ordered structure on Au(111) without cross-linking among nearest neighbors.[30] In air or water, where thiols exhibit little solubility, most of the displaced molecules often remain weakly attached to the gold substrate or SAMs in nearby locations. Therefore, the displacement is mostly reversible and cannot be used to pattern thiol SAMs.[31] Using solvents in which thiols exhibit sufficient solubility such as ethanol or 2-butanol, sharp patterns can be produced. Figure 3A shows a 50 × 50 nm^2 square hole within a C_{18}S/Au(111) layer produced in 2-butanol.

In contrast to thiol SAMs on gold, siloxane layers can be patterned using nanoshaving under various media.[27] Unlike thiol SAMs on gold, siloxane layers on mica do not exhibit long-range order.[27,32] There are very few covalent bonds between the siloxane molecules and the mica substrate due to the low density of dangling hydroxyl groups on the mica surface.[27,32] The stability of siloxane SAMs arises from the cross-linking of the chains through the Si−O network, which are formed by baking the adsorbate layer at 120 °C for 2 h.[27,32] Due to the low reactivity between the displaced siloxane molecules and mica, the displacement is irreversible, regardless of the fabrication medium. Siloxane molecules are either removed farther away from the fabrication sites during the scan, or they become attached to the AFM tip.[33] Figure 3B shows a "nanoheart" within an OTE/mica layer produced in air.

Nanografting. Nanografting can create both positive and negative patterns, depending upon the relative chain length between the new and matrix adsorbates.[20,28] Figure 4A displays two C_{18}S nanoislands fabricated into a matrix of C_{10}S/Au(111). It is important to point out that the newly

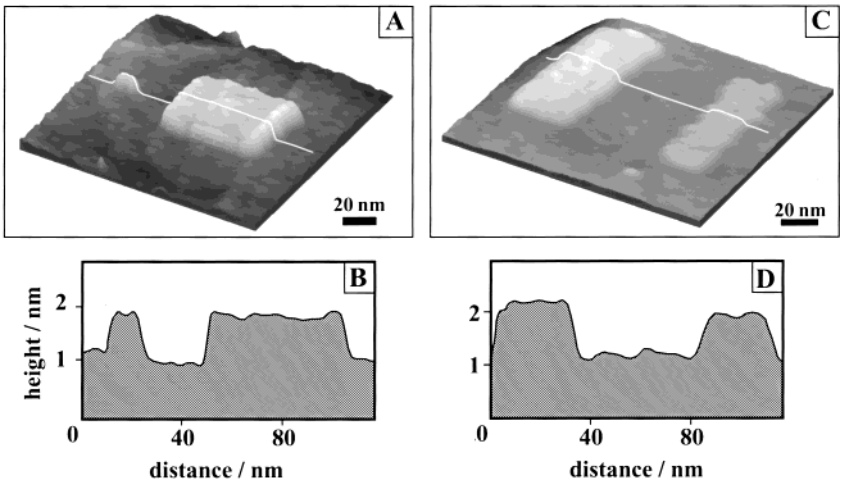

FIGURE 4. (A) Fabrication of two $C_{18}S$ nanoislands (3×5 and 50×50 nm^2) in the matrix of a $C_{10}S$ monolayer using nanografting. As shown in the cursor profile (B), the $C_{18}S$ islands are 8.8 Å higher than the surrounding $C_{10}S$ monolayer, consistent with the theoretical value for crystalline-phase SAMs. (C) Fabrication of multicomponent patterns using nanografting. The dimensions of the $C_{22}S$ (left) and $C_{18}S$ (right) islands are 30×60 and 20×60 nm^2, respectively. (D) The corresponding cursor profile shows that the $C_{18}S$ and $C_{22}S$ islands are 7.5 ± 1.0 and 12.0 ± 1.5 Å taller than the $C_{10}S$/Au matrix monolayer, respectively.

grafted $C_{18}S$ nanoislands not only have an ordered and close-packed $(3^{1/2} \times 3^{1/2})R30°$ lattice but also have fewer defects such as pinholes or uncovered areas.[20,28] During the time frame of nanofabrication experiments (hours to tens of hours), there were no observable exchange or desorption reactions.[20,28] The absence of pinhole defects and exchange reactions is critical for a faithful pattern transfer when patterned SAMs are used as masks. Using the same procedure, thiols with various chain lengths from 2 to 37 carbons (C_2SH, C_6SH, $C_{16}SH$, $C_{22}SH$, and $C_{18}OC_{19}SH$) have been successfully patterned.[28] The observed heights and high-resolution images of these nanopatterns indicate that the thiols are close-packed within the patterns. In addition, nanopatterns terminated with various functional groups such as $-OH$, $-CO_2H$, $-NH_2$, and $-CHO$ have also been produced.[28,34]

By changing thiol solution above the matrix layer before each nanografting experiment, we were able to produce multiple nanopatterns with desired arrangements and compositions of thiols. Figure 4C shows two patterns of different heights. First, a rectangular $C_{18}S$ pattern (20×60 nm^2) was grafted within a $C_{10}S$ matrix SAM. The solution was then replaced with a 0.2 mM $C_{22}SH$ solution, and a second rectangular pattern (30×70 nm^2) of $C_{22}S$ was grafted to the left of the $C_{18}S$ island. The $C_{18}S$ and $C_{22}S$ patterns were parallel to each other and were 0.80 ± 0.05 and 1.17 ± 0.03 nm taller than the surrounding $C_{10}S$ matrix (Figure 4D), respectively. Molecular resolution images of the two nanoislands revealed a hexagonal lattice with a lattice constant of 0.50 nm. Together, the height measurements and molecular resolution images indicated that the chains were closely packed within the nanoislands. The ability to produce multiple patterns regiospecifically from different adsorbates satisfies a basic requirement for fabrication of various nanoelectronic devices and sensor arrays.

In Situ Modification of SAM Nanopatterns. The unique advantage of nanografting is its ability to systematically change the patterns in situ without restarting of the entire fabrication process.[28] In Figure 5, two parallel $C_{18}S$ nanolines (10×50 nm^2) were first produced in a $C_{10}S$ matrix with a separation of 20 nm. The interline separation was then increased to 65 nm.[28] To perform this operation, we erased the right line by scanning the area defining this line at a high force in a $C_{10}SH$ solution. After the line on the right was erased, we then replaced the $C_{10}SH$ solution with a $C_{18}SH$ solution and fabricated a new line further to the right of the first $C_{18}S$ line, thereby increasing the interline spacing to 65 nm. In contrast to other microfabrication methods, the use of nanografting to modify a prepared pattern does not require the generation of new masks or a repeat of an entire fabrication process. This ability to interactively pattern on the nanometer scale provides a unique opportunity for studying size-dependent properties systematically and unambiguously as all other experimental conditions can be held constant.

Nanofabrication of SAMs with Tunneling Electrons. Previous studies have shown that STM images of SAMs with true molecular resolution are achieved at low tunneling current (1−100 pA) and under UHV.[21,22] STM images allow thiol SAMs to be visualized with unprecedented detail, such as the primary $(3^{1/2} \times 3^{1/2})R30°$ structure, the $c(4 \times 2)$ superlattice, and various defects including etch pits, domain boundaries, steps, and valleys on the gold substrate.[21,22]

An example of the STM image is shown in Figure 6A, in which ordered decanethiol domains with various orientations are visible. These domains are separated by boundaries and etch pits. True molecular resolution is demonstrated in Figure 6B, which displays the ordered structure of a $C_{10}S$/Au and the molecular defects at the domain boundary. At 70 pA, an L-shaped pattern, 10 nm in width, was produced (Figure 6C). The pattern is 0.7 nm lower than the surrounding SAM (see cursor profile in Figure 6D). The apparent depth is deeper than the single Au(111) step but smaller than the chain length of the

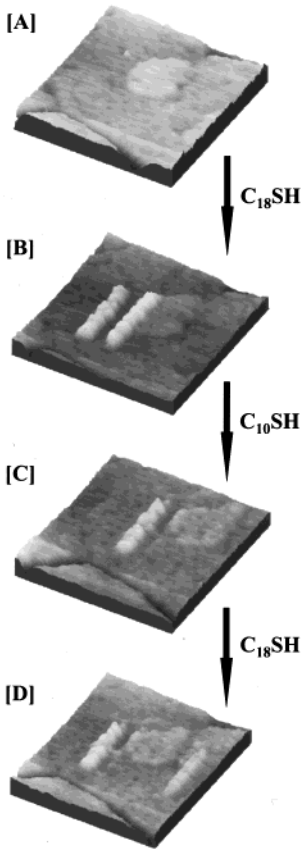

FIGURE 5. In situ modification of the grafted nanostructures. (A) AFM image of the matrix $C_{10}S$ SAM before fabrication. The bright area that is 30 nm in diameter and 0.25 nm higher than the rest of the surface is due to a single atomic step of Au(111) covered by the $C_{10}S$ SAM. (B) After fabrication of two parallel $C_{18}S$ nanolines with dimensions of 10 × 50 nm^2 and a separation of 20 nm. (C) Erasure of the right line by scanning its area under a high imaging force in a $C_{10}SH$ solution. (D) Refabrication of the second line by scanning under a high imaging force in $C_{18}SH$ solution. The interline spacing was increased to 65 nm. The spatial precision for this fabrication is 2 nm.

decanethiol (1.4 nm). This is consistent with the previous STM studies and the fact that alkyl chains do not make a significant contribution to the tunneling current.[21,22] The electronic density of states of hydrocarbon chains is sufficiently far from the Fermi levels of the tungsten tip and the gold substrate.[35,36] High-resolution images revealed the lack of periodicity of SAM within the nanopattern. Together the depth measurements and the high-resolution studies suggest the removal of thiols under the high tunneling current.

After tens of imaging and fabrication scans, the STM tip became covered with thiol molecules and other adsorbates. High-resolution images could still be obtained using these "aged tips", as shown in Figure 7A. However, the results of fabrication appeared to be dramatically different under conditions similar to those used in the generation of Figure 6. As shown in Figure 7B, a nearly triangular pattern was produced at 80 pA. However, thiols within this pattern were not removed as the $(3^{1/2} \times 3^{1/2})R30°$ structure still remained. The height difference between the pattern and the surrounding area is 0.24 nm

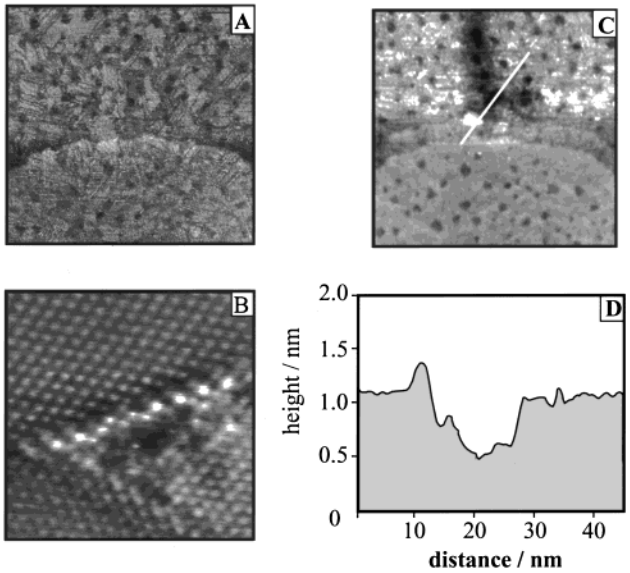

FIGURE 6. Example of tunneling electron-induced evaporation of thiols in $C_{10}S$/Au(111). (A) Constant-current STM topograph (100 × 100 nm^2) acquired at a bias voltage of 2 V and tunneling current of 4 pA. (B) A 7 × 7 nm^2 image reveals the packing and defects of the SAM with molecular resolution. (C) After an L-shaped area was scanned at 80 pA. (D) Cursor plot indicates that the depth of the pattern is 0.75 nm, and a new nanoisland near the patterned area is 0.24 nm higher than the matrix.

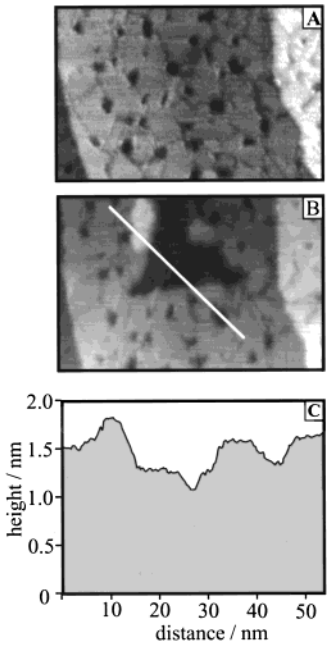

FIGURE 7. Example of tunneling electron-induced diffusion in $C_{10}S$/Au(111). (A) A 75 × 50 nm^2 constant-current STM topograph taken using a tungsten tip at 1.5 V and 6.6 pA. (B) After a triangular area was scanned at 80 pA. At this current, one layer of gold atoms under the SAM in the triangular area was displaced. (C) The cursor profile indicates that the central triangular area is 0.24 nm lower than the surrounding areas. The depth corresponds well with the single atomic height of Au(111).

(Figure 7C), corresponding well with a Au(111) step. The displaced gold atoms moved to the upper left part of the pattern (Figure 7B) and step edges. In other words, we can produce etch pits and nanoislands. It is known that

the number of etch pits may be reduced or eliminated by a mild annealing process, e.g., at 50 °C for 3 h.[21,37] Therefore, by combining annealing and our STM lithography, one can actively control the distribution and locations of etch pits within thiol SAMs by rearranging the gold atoms underneath the thiol SAM.

We may envision several possible fabrication mechanisms based on knowledge of STM tip−SAM interactions. Under our fabrication conditions, e.g., 2 V and 70 pA, STM tips penetrated into the SAM and located in close proximity to the Au−S interface. Under a very high local field (10^8−10^9 V/cm), an ultrasmall yet high-density electron beam was directed by the tip to collide with the S−Au interface. The S−Au bonds (40 kcal/mol) were most likely weakened or broken under such high tunneling current.[38] With the presence of clean W or Pt−Rh tips, the thiols loosely bonded to gold surface could become attached to the tips. When these relatively "dirty" tips were used to fabricate SAMs, thiols had low affinity toward the tip and thus were not detached from the surface. At high current, the tunneling electrons exciteed the top layer of gold atoms after the Au−S bonds were broken, causing the lateral displacement of gold atoms. Tips may be cleaned again using voltage pulsing (negative 2−5 V for 10 ms) to deposit adsorbed materials from the tip to the surface.[25,39,40]

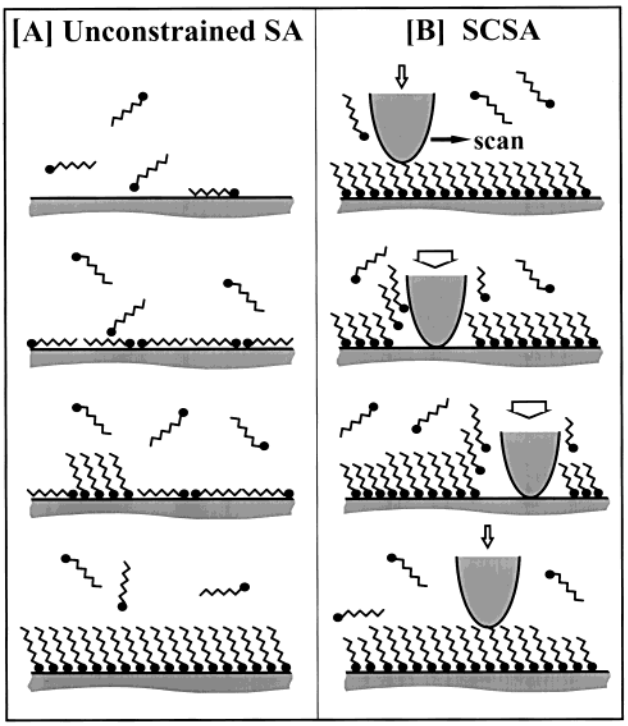

FIGURE 8. Schematic diagram showing the reaction pathway for the (A) unconstrained and (B) spatially constrained self-assembly (SCSA) reactions.

Applications of SPL and Patterned SAMs

Changing the Microenvironment of Surface Reactions. During nanografting, the top asperity of the AFM tip displaces adsorbed thiols within the matrix SAM, thus producing a transient reaction environment in which the newly exposed gold surface is spatially confined by surrounding thiols and the AFM tip. At least one order of magnitude increase in the reaction rate was observed for the self-assembly of *n*-alkane thiols under spatial confinement with respect to the corresponding unconstrained processes.[20] In addition, the resulting SAMs formed under spatial confinement do not have "scars" or uncovered areas.

The accelerated kinetics and the resulting scar-free layer can be explained qualitatively by an altered reaction pathway, as schematically shown in Figure 8. It is known from SPM[35,41] and diffraction studies[42] that unconstrained self-assembly includes two main steps. Molecules initially attach to gold with their axis parallel to the surface, forming a lying-down phase as a reaction intermediate (Figure 8A). As the reaction proceeds, thiols stand up and eventually form a complete layer.[35,41,42] During nanografting, an AFM tip exposes a bare gold surface within a previously assembled monolayer. The newly exposed gold is spatially confined by the tip and surrounding thiols. Such spatial confinement restricts the formation of a lying-down configuration for adsorbing thiols but favors their direct adoption of the standing-up configuration.[20] Thus, the self-assembly process follows a pathway that bypasses the lying-down to standing-up transition (Figure 8B).

This standing-up configuration facilitates the ligation of sulfur to gold and the packing of the chains to form the SAM. In addition, the standing-up configuration is also enthalpically favorable because the interactions between the newly adsorbed molecules and the surrounding thiols help stabilize the transition states for the self-assembly process. Thus, the overall activation energy for the spatially confined self-assembly (SCSA) is most likely lower than that in the unconstrained reaction process. As a result, self-assembly on the constrained gold surfaces proceeds with a faster reaction rate. The accelerated kinetics are critically dependent on the dimension of the spatial confinement, with exposed surface dimensions less than the chain length of the adsorbing thiols appearing to prevent alternative reaction paths most efficiently.[20]

The proposed model is analogous to the accelerated kinetics observed within the cavities of zeolites and the capsules of certain supramolecular complexes.[43] This finding has generic implications in that spatial confinement can provide an effective means for changing the mechanism of certain surface reactions by sterically hindering alternative pathways and for accelerating the kinetics of a surface reaction by stabilizing particular transition states or reaction intermediates.

Direct Characterization of AFM Tip and Tip−Surface Contact. In SPM imaging as well as fabrication, the sharpness of the very top portion of the tip is most critical. The power of AFM also lies in its capability to simultaneously image local topography and physical properties such as elastic compliance, frictional force, and conductivity.[26,44,45] The quantification of this these properties requires the tip size and the tip−surface contact area to be known.[26,44,45] There is, however, no direct and easy way to characterize the top portion of the tips. The diameter

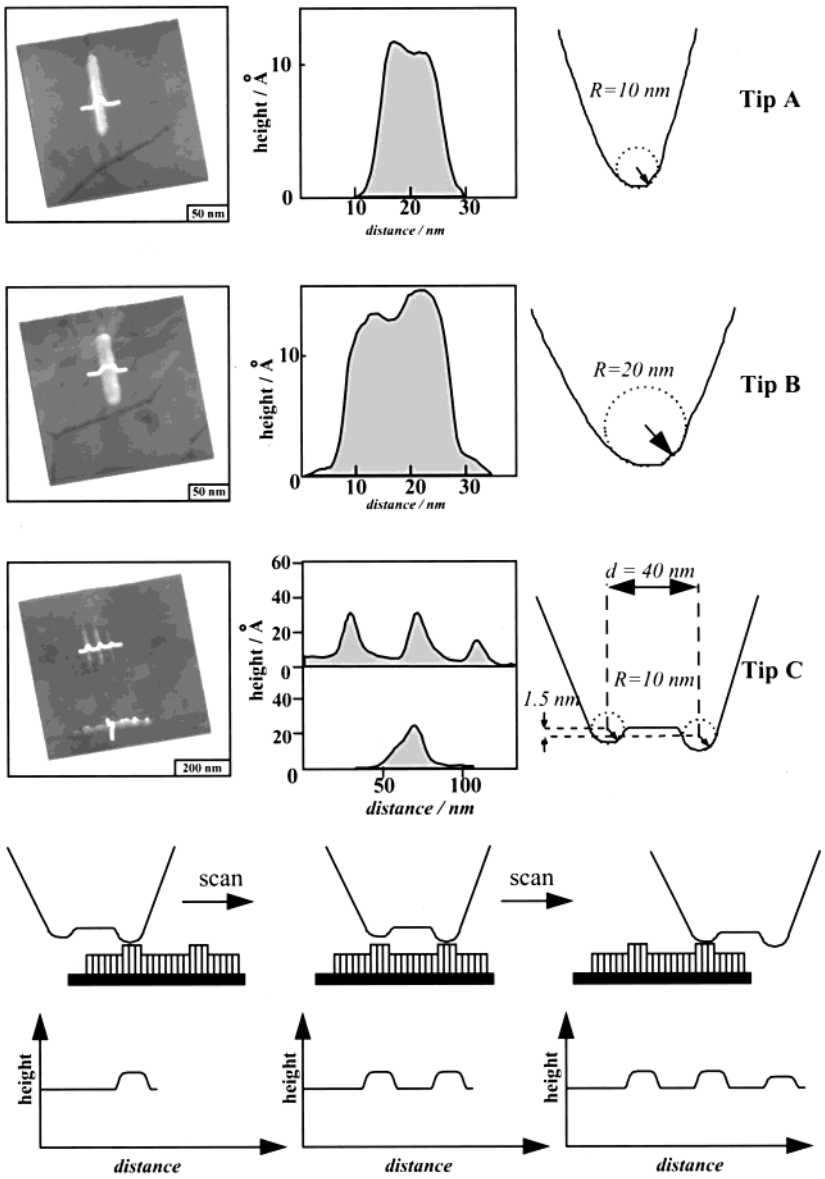

FIGURE 9. Characterization of three AFM tips using nanografting. In the top three rows, the topographic images and corresponding cursor plots are shown in the left and middle columns respectively, and the schematics of the tips are shown on the right column. The bottom two rows explain the convolution of tip C in AFM imaging.

of the tips is estimated from the topographic images of surface steps with known heights.[46] The choices typically include crystalline steps such as Au(111), C(0001), or mica (0001).

Nanografting provides a new and direct method to characterize AFM tips and contact areas. First, only a single scan is taken at a high load, and then the resulting line is imaged at a low imaging force. For the three tips shown in Figure 9, a single scan by each tip resulted in a narrow line, a wide line, and a triple-line pattern, respectively. The lines shown in Figure 9 consist of $C_{22}SH$ and thus are 12 Å taller than the matrix $C_{10}S/Au(111)$ layer. Since thiols are closely packed within the grafted patterns,[28] these lines have sharp and straight edges. Information about the top asperity of the AFM tips can then be extracted from the corresponding topographic images: (i) the cursor profile at both edges of each line (width w and height h) reflects the local shapes of the AFM tip [$R = (w^2 + h^2)/2h$]; (ii) the flat portion of the line corresponds to the lower limit of the contact diameter; and (iii) the measured overall width of the line represents the upper limit of the tip diameter because of the tip convolution.

In Figure 9, tips A and B have a single asperity at the top with a radius of 10 and 20 nm, respectively. The minimum contact diameter during fabrication is 6 nm for tip A and 9 nm for tip B. The third tip (tip C) has double asperities at the top. Multiple asperities occur frequently in SPM, yet they are difficult to quantify. Using nanografting, tips with multiple asperities can be identified and quantified directly. In the case of tip C, the AFM image reveals a triplet line and a single line after a y-scan and an x-scan, respectively. Thus, the doublet in tip C is aligned along the x-direction. The rationale behind this conclusion is illustrated schematically in Figure 9. A doublet tip scanning over a pair of parallel lines with the

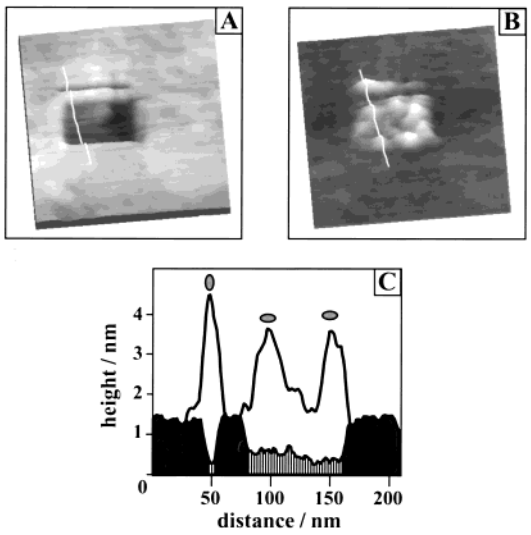

FIGURE 10. Formation of two nanopattens of LYZ. (A) A 400 × 400 nm^2 topographic image of a $C_{10}S$/Au(111) SAM, within which a 10 × 150 nm^2 line and a 100 × 150 nm^2 rectangle of $HS(CH_2)_2COOH$ were produced using nanografting. (B) The same area imaged after 4 min of immersion in a LYZ solution (10 μg/mL in 20 mM HEPES buffer, pH = 7.0). (C) Corresponding cursor profiles in one plot. The origin is the gold surface, which can be determined by displacing the SAM. The black and striped regions represent the matrix and nanopatterned SAMs, respectively. Each peak corresponds to a one adsorbed LYZ molecule.

same separation would result in a triplet line in the AFM image. The dimensions of this double tip are also extracted directly from the corresponding peak widths and separation in the cursor profiles. The two asperities in tip C are 10 nm in radius separated by 40 nm. In addition, the left asperity is 1.5 nm shorter than the right one.

By systematic varyation of the chain length of thiols in the matrix and solution, lines with heights ranging from 2 to 45 Å have been produced, which provides more choices of the step heights than commonly used crystalline steps such as mica (0001). Nanografting provides a direct and rapid method to estimate the contact diameter and three-dimensional geometry of AFM tips, in addition to the tip radius, regardless of single or multiple asperities.

Production of Nanometer-Sized Protein Patterns. Patterned SAMs produced using SPL may be used as templates for subsequent fabrication processes such as patterning proteins by selective adsorption.[34] Selectivity of protein adsorption can be achieved with the knowledge of the variation in protein affinity toward different SAMs.[4,47−51]

As a proof-of-concept experiment, we first patterned lysozyme (LYZ), an enzyme that catalyzes the hydrolysis of the glycosidic links between GlcNAc and MurNAc residues in the polysaccharide.[34] As shown in Figure 10A, two $HS(CH_2)_2COOH$ nanopatterns, a line and a rectangle, were first grafted within a matrix $C_{10}S$/Au. The patterning and imaging of SAMs were conducted in an aqueous medium containing 1 mM $HS(CH_2)_2COOH$. Prior to protein adsorption, the patterned SAM was first washed with deionized water to remove any remaining $HS(CH_2)_2COOH$ and then washed with 20 mM HEPES buffer (pH 7.0). After injection of a 10 μg/mL LYZ solution, proteins adsorbed exclusively onto the two HOOC-terminated areas within 3 min, as shown in Figure 10B. Little adsorption was observed at the methyl-terminated areas during the experiment (4 h). The observed strong selectivity is mainly attributed to the electrostatic interaction between LYZ and the surface of $HOOC(CH_2)_2S$/Au(111).[4,34,51] At neutral pH, LYZ (IEP 11.1) exhibits net positive charges, while ~10% of the carboxylate termini are negatively charged ($-COO^-$).[52] Therefore, electrostatic attraction drives the selective adsorption of LYZ onto the HOOC-terminated areas instead of the methyl-terminated matrix.

Individual LYZ particles within the patterns can be resolved from the AFM image shown in Figure 10B. The corresponding cursor profiles shown in Figure 10C reveal that the immobilized protein molecules exhibit different heights: 4.3 ± 0.2 and 3.0 ± 0.2 nm. LYZ molecules are ellipsoidal with dimensions about 4.5 × 3.0 × 3.0 nm^3 from X-ray crystallographic studies.[53] The variation in heights shown in Figure 10 is consistent with the fact that electrostatic interactions are not specific and often result in various protein orientations with respect to the surface.[4,51,54] The advantage of using this physically mediated protein immobilization is the experimental simplicity. In addition, proteins retain their activity after the adsorption.[51,55,56] We have succeeded in patterning other proteins including BSA and IgG using either electrostatic interaction or covalent binding between the primary amine in the protein residues (such as lysine) and the surface aldehyde groups of the SAMs.[34] The patterns range from 15 nm to 1 μm in lateral dimension.[34]

Conclusion and Future Outlook

We have developed several SPL-based methods to produce nanometer-sized patterns within SAMs. The key to achieving high spatial precision is to keep the tip−surface interactions strong and local. In this Account, we introduced two AFM-based methods, nanoshaving and nanografting, which rely on the local force, and two STM-based techniques, electron-induced diffusion and desorption, which use tunneling electrons for fabrication. Compared with other techniques used to fabricate microstructures of SAMs, SPL, especially STM-based lithography, offers the highest spatial precision. While our STM lithography is carried out in UHV, the AFM fabrication can be done in an ambient environment and is relatively simple to set up. Edge resolution of several nanometers is routinely obtained, and molecular precision can be achieved with an ultrasharp tip. In addition, nanostructures can be characterized with molecular resolution in situ using the same tip. Using nanografting, one can also quickly change and/or modify the fabricated patterns in situ without changing the mask or repeating the entire fabrication procedure. Various examples discussed in this Account demonstrate that SPL can be used as a generic method for nanofabrication of SAMs. In addition, the SPL process itself allows many new phenomena to be revealed and studied, such as spatially confined reactions. In combina-

tion with protein immobilization techniques, we used SPL to produce nanometer-sized protein patterns.

In light of the initial success, much more work lies ahead. A well-known limitation of all SPL procedures is that the fabrication steps are serial instead of parallel in nature, which results in a relatively low fabrication speed. Therefore, at present, SPL is used as a research tool in laboratories instead of as a manufacturing tool for high-throughput applications. In addition, more pattern-transfer protocols such as selective etching and deposition also need to be tested to explore the feasibility of using SPL to produce nanostructures of metals and semiconductors. Furthermore, the ability to change nanostructures in situ provides a unique opportunity for systematic studies of size-dependent properties of nanostructures in the near future.

The strength of our approach is the ability to engineer and image complex molecular architectures with high spatial precision. The precisely engineeered nanostructures allow for the exploration of chemical and biochemical reactions under spatially well-defined and controlled environments. Although not yet practical for high-throughput applications and manufacturing, SPL studies provide fundamental infromation on tip−surface interactions, structures, and properties on a nanoscopic level. These studies shall serve as a useful guide in the nanofabrication of nanoelectronic devices, biosensors, and biochips.

We thank Professor Paul E. Laibinis at MIT for the $CH_3(CH_2)_{21}$-SH compound. We appreciate many helpful discussions with Kapila Wadu-Mestrige, Jayne Garno, Nabil Amro, Yan Huang, and Bill Price at WSU. S.X. and Y.Q. thank WSU for a Rumble and IMR fellowship, respectively. G.Y.L. gratefully acknowledges the Camille and Henry Dreyfus Foundation for a New Faculty Award, and the Arnold and Mabel Beckman Foundation for a Young Investigator Award. This work is also supported by the National Science Foundation (Grant CHE-9733400), The Whitaker Foundation (Biomedical Engineering Grant), and the Petroleum Research Fund (Type-AC).

References

(1) Bishop, A.; Nuzzo, R. G. Self-assembled Monolayers: Recent Developments and Applications. *Curr. Opin. Colloid Interface Sci.* **1996**, *1*, 127.

(2) Kumar, A.; Abbott, N. L.; Kim., E.; Biebuyck, H. A.; Whitesides, G. M. Patterned Self-assembled Monolayers and Mesoscale Phenomena. *Acc. Chem. Res.* **1995**, *28*, 219.

(3) Bumm, L. A.; Arnold, J. J.; Cygan, M. T.; Dunbar, T. D.; Burgin, T. P.; Jones, L.; Allara, D. L.; Tour, J. M.; Weiss, P. S. Are single molecular wires conducting? *Science* **1996**, *271*, 1705.

(4) (a) Mrksich, M.; Whitesides, G. M. Using Self-assembled Monolayers to Understand the Interactions of Man-made Surfaces with Proteins and Cells. *Annu. Rev. Biophys. Biomol. Struct.* **1996**, *25,* 55. (b) Bernard, A.; Delamarche, E.; Schmid, H.; Michel, B.; Bosshard, H. R.; Biebuyck, H. Printing Patterns of Proteins. *Langmuir* **1998**, *14*, 2225.

(5) (a) Huang, J. Y.; Dahlgren, D. A.; Hemminger, J. C. Photopatterning of Self-assembled Alaknethiolate monolayers on Gold−A Simple Monolayer Photoresist Utilizing Aqueous Chemistry. *Langmuir* **1994**, *10*, 626. (b) Tarlov, M. J.; Burgess, D. R. F.; Gillen, G. UV Photopatterning of Alkanethiolate Monolayers Self-assembled on Gold and Silver. *J. Am. Chem. Soc.* **1993**, *115*, 5305. (c) Wollman, E. W.; Kang, D.; Frisbie, C. D.; Lorkovic, I. M.; Wrighton, M. S. Photosensitive Self-assembled Monolayers on Gold: Photochemistry of Surface-Confined Aryl Azide and Cyclopentadienylmanganese Tricarbonyl. *J. Am. Chem. Soc.* **1996**, *116*, 4395.

(6) Abbott, N. L.; Kumar, A.; Whitesides, G. M. Using Micromachining, Molecular Self-assembly, and Wet Etching to Fabricate 0.1−1-μm-Scale Structures of Gold and Silicon. *Chem. Mater.* **1994**, *6*, 596.

(7) Tiberio, R. C.; Craighead, H. G.; Lercel, M.; Lau, T.; Sheen, C. W.; Allara, D. L. Self-assembled Monolayer Electron-Beam Resist on GaAs. *Appl. Phys. Lett.* **1993**, *62*, 476.

(8) Xia, Y.; Whitesides, G. M. Use of Controlled Reactive Spreading of Liquid Alkanethiol on the Surface of Gold to Modify the Size of Features Produced by Microcontact Printing. *J. Am. Chem. Soc.* **1995**, *117*, 3274.

(9) (a) Sondag-Huethorst, J. A. M.; Van Helleputte, H. R. J.; Fokkink, L. G. J. Generation of Electrochemically Deposited Metal Patterns By Means of Electron-Beam Lithography of Self-assembled Monolayer Resists. *Appl. Phys. Lett.* **1994**, *64*, 285. (b) Berggren, K. K.; et al. Microlithography by Using Neutral Metastable Atoms and Self-assembled Monolayers. *Science* **1995**, *269*, 1255.

(10) (a) Offord, D. A.; John, C. M.; Linford, M. R.; Griffin, J. H. Contact-angle Goniometry, Ellipsometry, and Time-of-flight SIMS of Gold Supported Mixed SAMs Formed from Alkyl Mercaptans. *Langmuir* **1994**, *10*, 883. (b) Tamada, K.; Hara, M.; Sasabe, H.; Knoll, W. Surface Phase Behavior of n-alkanethiol Self-Assembled Monolayers Adsorbed on Au(111): An AFM Study. *Langmuir* **1997**, *13*, 1558.

(11) (a) Hayes, W. A.; Kim, H.; Yue, X.; Perry, S. S.; Shannon, C. Nanometer-scale Patterning of Surfaces Using Self-assembly Chemistry 2. *Langmuir* **1997**, *13*, 2511. (b) Bilewicz, R.; Sawaguchi, T.; Chamberlain, R. V.; Majda, M. Monomolecular Langmuir−Blodgett Films at Electrodes: Electrochemistry at Single-Molecule Gate Sites. *Langmuir* **1995**, *11*, 2256.

(12) Binnig, G.; Rohrer, H.; Gerber, Ch.; Weibel, E. Surface Studies by Scanning Tunneling Microscopy. *Phys. Rev. Lett.* **1982**, *49*, 57.

(13) Binnig, G.; Quate, C. F.; Gerber, Ch. Atomic Force Microscope. *Phys. Rev. Lett.* **1986**, *56,* 930.

(14) There are many excellent books and review articles regarding SPM. Here we list four examples: (a) Chen, C. J. *Introduction to Scanning Tunneling Microscopy*; Oxford University Press: New York, 1993. (b) Sarid, D. *Scanning Force Microscopy, with applications to electric, magnetic and atomic forces*; Oxford University Press: New York, 1991. (c) Frommer, J. STM and AFM in Organic Chemistry. *Angew. Chem., Int. Ed. Engl.* **1992,** *31,* 1298. (d) Hamers, R. J. Scanning Probe Microscopes in Chemistry. *J. Phys. Chem.* **1996**, *100*, 13103.

(15) (a) Eigler, D. M.; Schweizer, E. K. Positioning Single Atoms with a STM. *Nature* **1990**, *344*, 524. (b) Zeppenfeld, P.; Lutz, C. P.; Eigler, D. M. Manipulating Atoms and Molecules with a STM. *Ultramicroscopy* **1992**, *42−44,* 128. (c) Crommie, M. F.; Lutz, C. P.; Eigler, D. M. Confinement of Electrons to Quantum Corrals on a Metal-Surface. *Science* **1993**, *262*, 218. (d) Jung, T. A.; Schlittler, R. R.; Gimzewski, J. K.; Tang, H.; Joachim, C. Controlled Room-Temperature Positioning of Individual Molecules: Molecular Flexure and Motion. *Science* **1996**, *271*, 181.

(16) (a) Avouris, Ph. Manipulation of Matter at the Atomic and Molecular-Levels. *Acc. Chem. Res.* **1995**, *28*, 95. (b) Lyo, I.; Avouris, P. Field-induced Nanometer-scale to Atomic-scale Manipulation of Silicon Surfaces with the STM. *Science* **1991**, *253*, 173. (c) Salling, C. T.; Lagally, M. G. Fabrication of Atomic-scale Structures on Si(001) Surfaces. *Science* **1994**, *265*, 502. (d) Stipe, B. C.; et al. Single-Molecule Dissociation by Tunneling Electrons. *Phys. Rev. Lett.* **1997**, *78*, 4410.

(17) Nyffenegger, R. M.; Penner, R. M. Nanometer-scale Surface Modification Using the Scanning Probe Microscope: Progress Since 1991. *Chem. Rev.* **1997**, *97*, 1195.

(18) Ho, W. Inducing and Viewing Bond Selected Chemistry with Tunneling Electrons. *Acc. Chem. Res.* **1998**, *31*, 567.

(19) Butt, H. J.; Seifert, K.; Bamberg, E. Imaging Molecular Defects in Alkanethiol Monolayers with an AFM. *J. Phys. Chem.* **1993**, *97*, 7316.

(20) Xu, S.; Laibinis, P. E.; Liu, G.-Y. Accelerating the Kinetics of Thiol Self-assembly on Gold−A Spatial Confinement Effect. *J. Am. Chem. Soc.* **1998**, *120*, 9356.

(21) (a) Poirier, P. E.; Pylant, E. D.; White, J. M. Crystalline Structures of Pristine and Hydrated Mercaptohexanol Self-assembled Monolayers an Au(111). *J. Chem. Phys.* **1996**, *105*, 2089. (b) Poirier, P. E.; Tarlor, M. J. The c(4×2) Superlattice of *n*-Alkanethiol Monolayers Self-assembled on Au(111). *Langmuir* **1994**, *10,* 2853. (c) McDermott, C. A.; McDermott, M. T.; Green, J. B.; Porter, M. D. Structural Origins of the Surface Depressions at Alkanethiolate Monolayers on Au(111)−A Scanning Tunneling and Atomic Force Microscopic Investigation. *J. Phys. Chem.* **1995**, *99*, 13257.

(22) (a) Delamarche, E.; Michel, B.; Biebuyek, H. A.; Gerber, C. Golden Interfaces: The Surface of Self-assembled Monolayers. *Adv. Mater.* **1996**, *8*, 719. (b) Weiss, P. S.; et al. Atomic Scale View of Motion on Surfaces. *Ann. Chim. Acta* **1995**, *307,* 355. (c) Kang,

J.; Rowntree, P. A. Molecularly Resolved Surface Superstructures of Self-assembled Butanethiol Monolayers on Gold. *Langmuir* **1996**, *12*, 2813. (d) Schonenberger, C.; Sondag-Hüthorst, J. A. M.; Jorritsima, J.; Fokkink, L. J. G. What Are The Holes In Self-assembled Monolayers of Alkanethiols on Gold? *Langmuir* **1994**, *10*, 611.

(23) Muller, W. T.; et al. A Strategy for the Chemical Synthesis of Nanostructures. *Science* **1995**, *268*, 272.

(24) Piner, R. D.; Zhu, J.; Xu, F.; Hong, S. H.; Mirkin, C. A. "Dip-pen" Nanolithography. *Science* **1999**, *283*, 661.

(25) Ross, C. B.; Sun, L.; Crooks, R. M.; Scanning Probe Lithography. 1. Scanning Tunneling Microscope Induced Lithography of Self-assembled N-Alkanethiol Monolayer Resists. *Langmuir* **1993**, *9*, 632.

(26) Carpick, R. W.; Salmeron, M. Scratching the Surface: Fundamental Investigations of Tribology with Atomic Force Microscopy. *Chem. Rev.* **1997**, *97,* 1163.

(27) (a) Xiao, X. D.; Liu, G. Y.; Charych, D. H.; Salmeron, M. Preparation, Structure, and Mechanical Stability of Alkylsilane Monolayers on Mica. *Langmuir* **1995**, *11*, 1600. (b) Kiridena, W.; Jain, V.; Kuo, P. K.; Liu, G. Y. Nanometer-scale Elasticity Measurements on Organic Monolayers using SFM. *Surf. Interface Anal.* **1997**, *25*, 383.

(28) (a) Xu, S.; Liu, G.-Y. Nanometer-scale Fabrication by Simultaneous Nanoshaving and Molecular Self-assembly. *Langmuir* **1997**, *13*, 127. (b) Xu, S.; Miller, S.; Laibinis, P. E.; Liu, G.-Y. Fabrication of Nanometer Scale Patterns within Self-Assembled Monolayers by Nanografting. *Langmuir* **1999**, *15,* 7244.

(29) (a) Salmeron, M. B.; Folch, A.; Neubauer, G.; Tomitori, M.; Ogletree, D. F.; Kolbe, W. Nanometer Scale Mechanical-Properties of Au(111) Thin-Films. *Langmuir* **1992**, *8*, 2832. (b) Salmeron, M.; Neubauer, G.; Folch, A.; Tomitori; M.; Ogletree, D. F.; Sautet, P. Viscoelastic and Electrical-Properties of Self-assembled Monolayers on Au(111) Films. *Langmuir* **1993**, *9*, 3600.

(30) (a) Nuzzo, R. G.; Allara, D. L. Adsorption of Bifunctional Organic Disulfides on Gold Surfaces. *J. Am. Chem. Soc.* **1983**, *105*, 4481. (b) Chidsey, C. E. D.; Liu, G. Y.; Rowntree, P.; Scoles, G. Molecular Order at the Surface of an Organic Monolayer Studied by Low-Energy Helium Diffraction. *J. Chem. Phys.* **1989**, *91* (7), 4421. (c) Fenter, P.; Eberhardt, A.; Eisenberger, P. Self-assembly of N-Alkyl Thiols as Disulfides on Au(111). *Science* **1994**, *266*, 1216.

(31) (a) Liu, G.-Y.; Salmeron, M. B. Reversible Displacement of Chemisorbed N-Alkanethiol Molecules on Au(111) Surface-An Atomic Force Microscopy Study. *Langmuir* **1994**, *10*, 367. (b) Liu, G.-Y.; Fenter, P.; Eisenberger P.; Chidsey, C. E. D.; Ogletree, D. F.; Salmeron, M. *J.* An Unexpected Packing of Fluorinated N−Alkane Thiols On Au(111)-A Combined Atomic Force Microscopy And X-Ray Diffraction Study. *Chem. Phys.* **1994**, *101*, 4301.

(32) (a) Ulman, A. *An Introduction to Ultrathin Organic Films—From Langmuir−Blodgett to Self-assembly*; Academic Press: San Diego, 1991. (b) Maoz, R.; Yam, R.; Berkovic, G.; Sagiv, J. In *Organic Thin Films and Surfaces: Directions for the Nineties*; Ulman, A., Ed.; Thin Films 20; Academic Press: Boston, 1995; p 41.

(33) Jaschke, M.; Butt, H.-J. Deposition of Organic Meterial by the Tip of a SFM. *Langmuir* **1995**, *11*, 1061.

(34) Wadu-Mesthrige, K.; Amro, N.; Xu, S.; Liu, G.-Y. Fabrication and Imaging of Nanometer-Sized Protein Patterns. *Langmuir* **1999**, *15*, 8580.

(35) Poirier, G. E.; Pylant, E. D. The Self-assembly Mechanism of Alkanethiols on Au(111). *Science* **1996**, *272*, 1145.

(36) (a) Zubragel, C.; et al. Electronic-structure of Alkane Chains—Complete One-dimensional Band Structures of the Valence States. *Chem. Phys. Lett.* **1994**, *219*, 127. (b) Karpfen, A. Ab Initio Studies on Polymers. V. *J. Chem. Phys.* **1981**, *75*, 238.

(37) (a) Bucher, J. P.; Santesson, L.; Kern, K. Thermal Healing of Self-assembled Organic Monolayers. *Langmuir* **1994**, *10*, 979. (b) Delamarche, E.; Michel, B.; Kang, H.; Gerber, C. Thermal Stability of SAMs. *Langmuir* **1994**, *10*, 4103. (c) Camillone, N.; et al. New Monolayer Phases of n-Alkane thiols Self-assembled on Au(111). *J. Chem. Phys.* **1994**, *101*, 11031.

(38) Chen, J.; et al. Placement of Conjugated Oligomers in an Alkanethiol Matrix by Scanning Probe Lithography. *Appl. Phys. Lett.* **1999**, *75*, 624.

(39) Kim, Y. T.; Bard, A. J. Imaging and Etching of Self-assembled n-octadecanethiol Layers on Gold with the STM. *Langmuir* **1992**, *8*, 1096. (b) Mizutani, W.; Ishida, T.; Tokumoto, H. Nanoscale Reversible Molecular Extraction from a Self-assembled Monolayer on Gold(111) by a STM. *Langmuir* **1998**, *14*, 7197.

(40) Mizutani, W.; Ohi, A.; Motomatsu, M.; Tokumoto, H. Field-evaporation of Gold by STM. *Appl. Surf. Sci.* **1995**, *87/88,* 398. (b) Chang, C. S.; Su, W. B.; Tsong, T. T. Field-evaporation between a Gold Tip and a Gold Surface in the STM Configuration. *Phy. Rev. Lett.* **1994**, *72*, 574.

(41) Xu, S.; Cruchon-Dupeyrat, S. J. N.; Garno, J. C.; Liu, G.-Y.; Jennings, G. K.; Yong, T. H.; Laibinis, P. E. In situ Studies of Thiol Self-assembly on Gold from Solution Using AFM. *J. Chem. Phys.* **1998**, *108*, 5002.

(42) Camillone, N.; Leung, T. Y. B.; Schwartz, P.; Eisenberger, P.; Scoles, G. Chain Length Dependence of the Striped Phases of Alkanethiol Monolayers Self-assembled on Au(111): an Atomic Beam Diffraction Study. *Langmuir* **1996**, *12*, 2737.

(43) (a) Tokunaga, Y.; Rebek, J. Chiral Capsules. 1. Softballs with Asymmetric Surfaces Bind Camphor Derivatives. *J. Am. Chem. Soc.* **1998,** *120*, 66. (b) Kang, J. M.; Rebek, J. Entropically Driven Binding in a Self-assembling Molecular Capsule. *Nature* **1996**, *382*, 239.

(44) Overney, R. M.; et al. Force Microscopy Study of Friction and Elastic Compliance of Phase-separated Organic Thin Films. *Langmuir* **1994**, *10*, 1281. (b) Radmacher, M.; Tillmann, R. W.; Gaub, H. E. Imaging Viscoelasticity by Force Modulation with the AFM. *Biophys. J.* **1993**, *64*, 735.

(45) (a) Leatherman, G.; et al. Carotene as a Molecular Wire: Conducting AFM. *J. Phys. Chem. B* **1999,** *103,* 4006. (b) Kelley, T. W.; Granstrom, E. L.; Frisbie, C. D. Conducting Probe AFM: a Characterization Tool for Molecular Electronics. *Adv. Mater.* **1999**, *11*, 261.

(46) (a) Markiewicz, P.; Goh, C. AFM Tip Deconvolution Using Calibration Arrays. *Rev. Sci. Instrum.* **1995**, *66*, 3186. (b) Ramirez-Aguilar, K. A.; Rowlen, K. L. Tip Characterization from AFM images of Nanometric Spherical Particles. *Langmuir* **1998**, *14*, 2562.

(47) (a) Norde, W.; Giesbers, M.; Pingsheng, H. LB Films of Poly-10, 12-pentacosadiyonic Acid as Substrates for Protein Adsorption. *Colloids Surf. B: Biointerfaces* **1995**, *5*, 255. (b) Buijs, J.; Btitt, D. W.; Vladimer, H. Human Growth Hormone Adsorption Kinetics and Conformation on SAMs. *Langmuir* **1998**, *14*, 335.

(48) Wagner, P.; Hegner, M.; Kernen, P.; Zaugg, F.; Semenza, G. Covalent Immobilization of Native Biomolecules onto Au(111) via N-hydroxysuccinimide Ester Functionalized SAMs for SPM. *Biophys. J.* **1996**, *70*, 2052.

(49) Patel, N.; et al. Immobilization of Protein Molecules onto Homogeneous and Mixed Carboxylate-Terminated Self-assembled Monolayers. *Langmuir* **1997**, *13*, 6485.

(50) Wadu-Mesthrige, K.; Amro, N. A.; Liu, G.-Y. Immobilization of Proteins on Self-assembled Monolayers. *Scanning*, in press.

(51) Browning-Kelley, M. E.; Wadu-Mesthrige, K.; Hari, V.; Liu, G.-Y. AFM Study of Specific Antigen/antibody Binding. *Langmuir* **1997**, *13*, 343.

(52) The pK_a value for $HOOC(CH_2)_2S$/Au is 8 according to the following: Hu, K.; Bard, A. Use of Atomic Force Microscopy for the Study of Surface Acid−base Properties of Carboxylic Acid-terminated Self-assembled Monolayers. *Langmuir* **1997**, *13*, 5114. The measured pK_a value for the HOOC groups within SAM is much higher than that for individual molecules in solution. Such an increase in pK_a is most likely due to the formation of hydrogen bonds among the nearest neighbor HOOC terminals.

(53) Blake, C. C.; et al. Structure of Hen Egg-white Lysozyme. *Nature* **1965**, *206*, 757.

(54) Thomas, N. H.; et al. Oriented, Active E. coli RNA Polymerase: an AFM Study. *Biophys. J.* **1999**, *76*, 1024.

(55) Mrksich, M.; et al. Controlling Cell Attachment on Contoured Surfaces with Self-assembled Monolayers of Alkanethiolates on Gold. *Proc. Natl. Acad. Sci. U.S.A.* **1996**, *93*, 10775.

(56) Mooney, J. F.; Hunt, A. J.; McIntosh, J. R.; Liberko, C. A.; Walba, D. M.; Rogers, C. T. Patterning of Functional Antibodies and other Proteins by Photolithography of Silane Monolayers. *Proc. Natl. Acad. Sci. U.S.A.* **1996**, *93,* 12287.

AR980081S